Supplementary Materials for

Photo-induced Ultralong Phosphorescence of Carbon Dots for Thermal-sensitive Dynamic Patterning

Yanfeng Liu[†], Xin Huang[†], Zuoji Niu[†], Dongni Wang, Huilin Gou, Qiaobo Liao, Kai Xi, Zhongfu An*, Xudong Jia**

[†]: These three authors contributed equally to the work.

Y. Liu, Dr. X. Huang, D. Wang, H. Gou, Q. Liao, Prof. K. Xi, Prof. X. Jia
School of Chemistry and Chemical Engineering
Nanjing University, 163 Xianlin Road, Nanjing, 210023, China
E-mail: xikai@nju.edu.cn; jiaxd@nju.edu.cn

Z.Niu, Prof. Z. An*
Key Laboratory of Flexible Electronics (KLOFE) & Institute of Advanced Materials (IAM)
Nanjing Tech University (NanjingTech), 30 South Puzhu Road, Nanjing, 211816, China
E-mail: iamzfan@njtech.edu.cn

Y. Liu, Prof. X. Jia*
State Key Laboratory of Coordination Chemistry, Nanjing National Laboratory of Microstructures
Nanjing University, 163 Xianlin Road, Nanjing, 210023, China
E-mail: jiaxd@nju.edu.cn

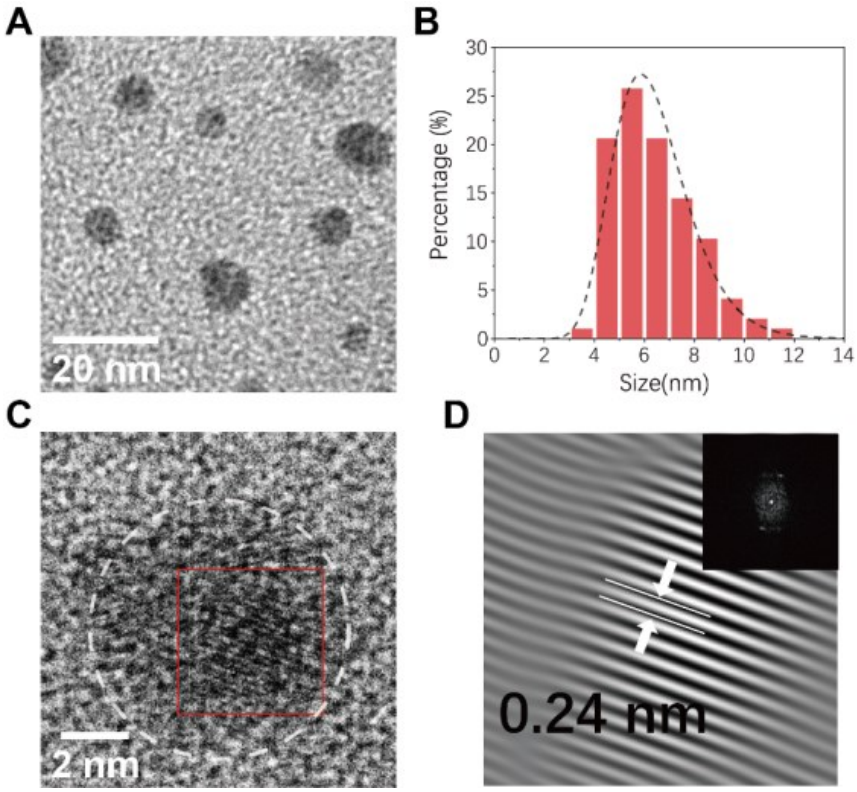

Fig. S1. The morphology of CDs revealed by TEM. (A) TEM image of CDs under 100,000x magnification. **(B)** Size distribution of CDs calculated from 97 individual dots. **(C)** TEM image of an individual PCD under 800,000x magnification, lattice fringes indicated that the dots were partially crystalline. **(D)** The Fourier-filtered image of the selected red square area. Inset: Fast Fourier Transform (FFT) from the red square labeled in c. The average stripe interval was 0.24 nm, corresponding to the [1 0 0] lattice plane of graphitic carbon.

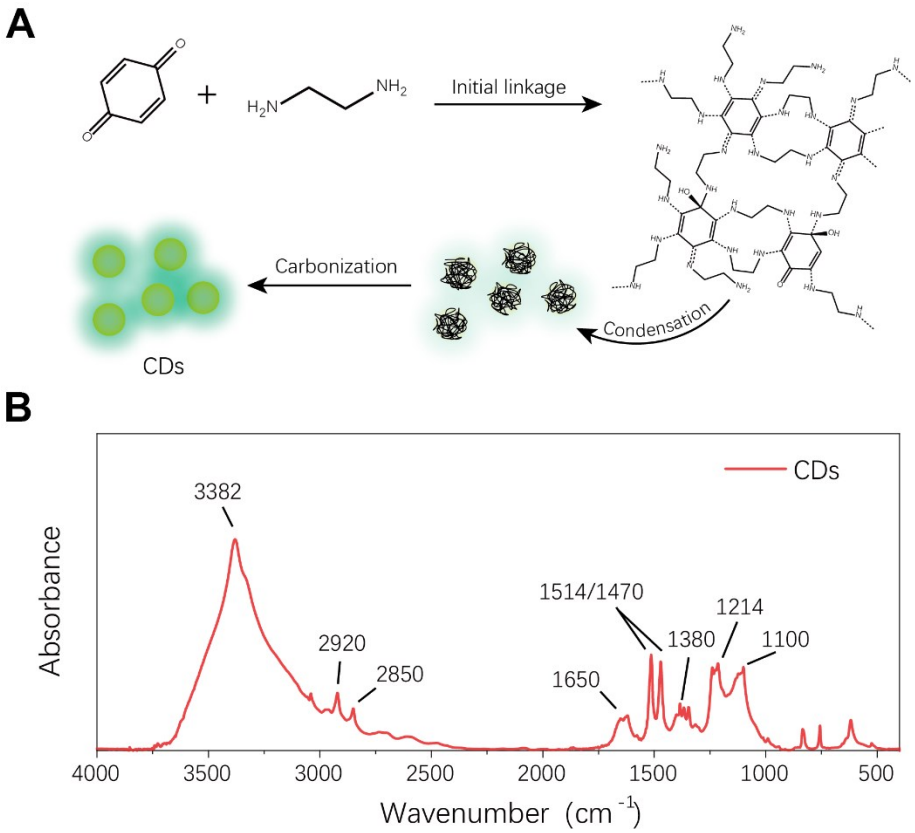

Fig. S2. The FT-IR spectra of the CDs. (A) Schematic illustration for the formation process of CDs. Two molecular precursors PBQ and EDA were used to prepare CDs under solvothermal condition. These two precursors were highly reactive, and capable of reacting through Michael addition pathway under heating conditions. Due to the high degree of functionality of both precursors (4~6 for PBQ and 2 for EDA), inter-locked crosslinking nano-structure subsequently formed through initial linkage and following condensation, which further carbonized under into the CDs. **(B)** Fourier transformed infrared (FT-IR) absorbance spectrum of the purified CDs.

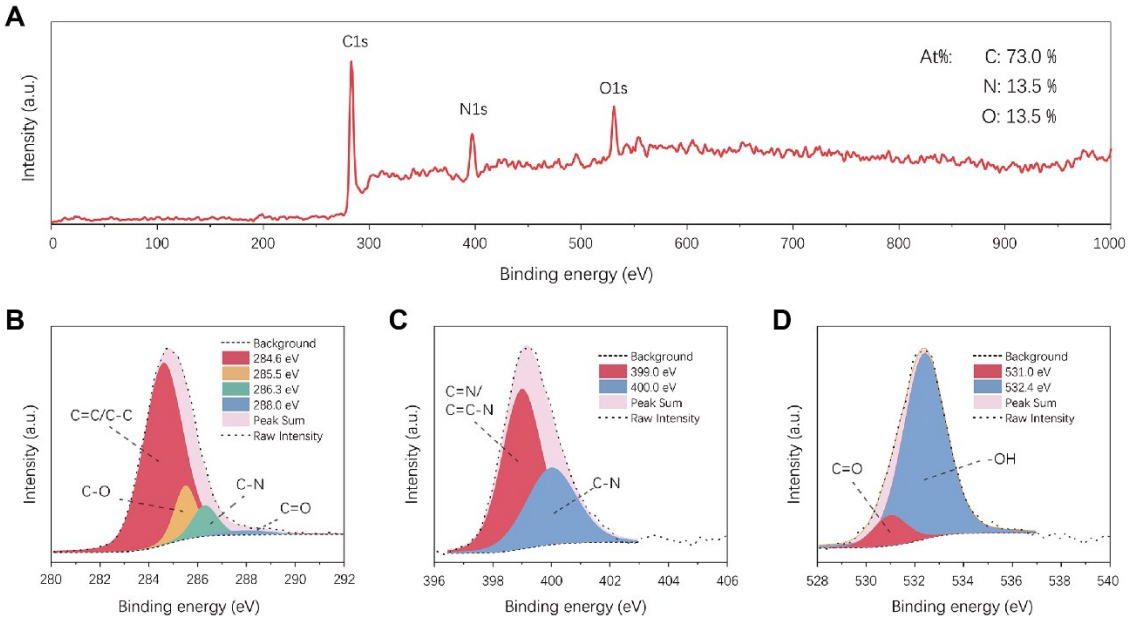

Fig. S3. The X-ray photoelectron spectra (XPS) data of CDs. (A) The XPS Survey. **(B)** The C1s binding energy and assignment. **(C)** The N1s binding energy and assignment. **(D)** The O1s binding energy and assignment. The values of binding energy have been calibrated according to adventitious carbon contamination (284.6 eV)

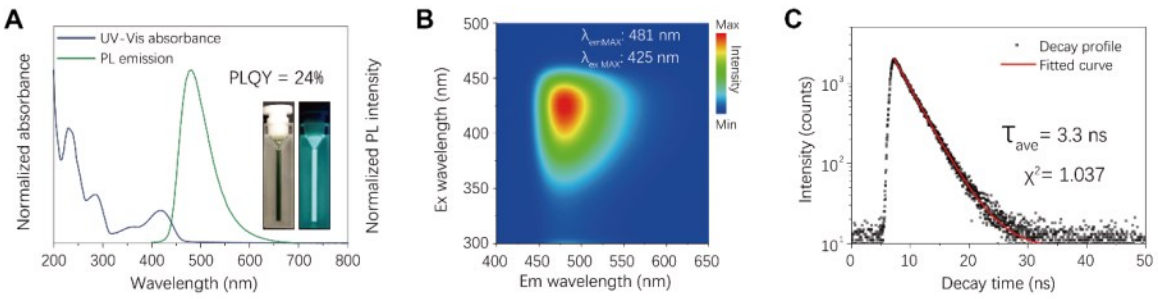

Fig. S4. The absorbance and PL features of CDs. (A) Normalized UV-Vis absorbance and PL emission spectra of CDs. The PLQY of CDs was determined by absolute method with an integrating sphere accessory. **(B)** Emission mapping of CDs with excitation range from 300 to 500 nm and emission range from 400 to 650 nm. Maximal PL intensity occurred at 425 nm excitation and 481 nm emission. CDs can also be efficiently excited with 400 nm irradiation, where 79.4% of maximal PL intensity maintained. **(C)** PL lifetime profile of CDs (Excitation wavelength: 400 nm, emission wavelength: 481 nm). A mono-exponential decay was recorded with an average PL lifetime of 3.3 ns.

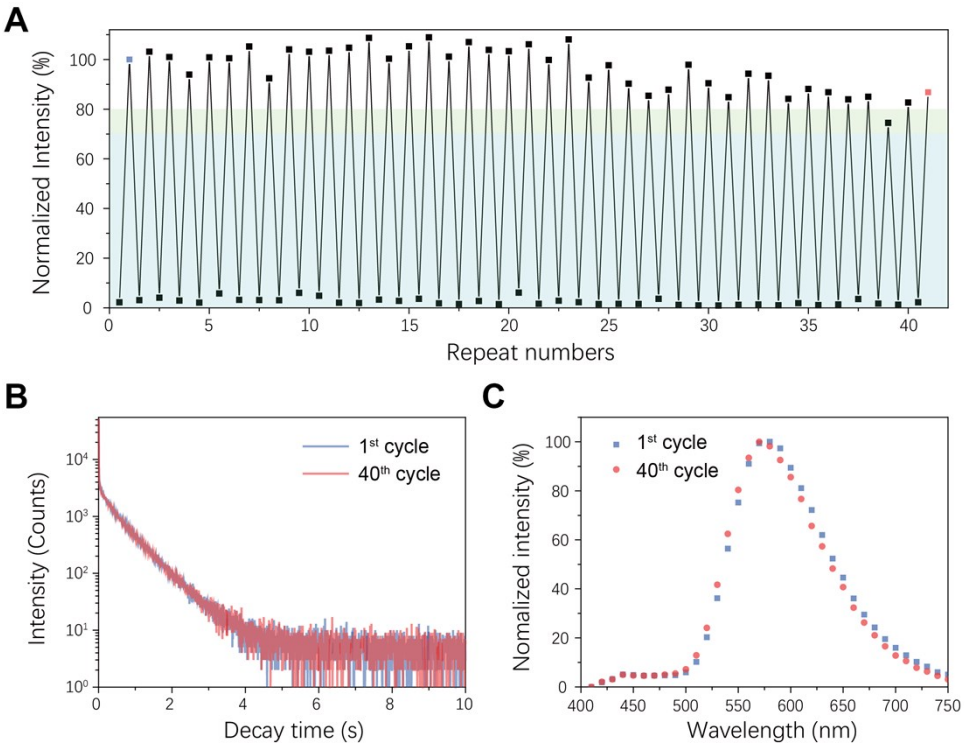

Fig. S5. Reversibility of the photo-induced URTP in CDs/PVP film. To evaluate the reversibility of the afterglow on/off switch, herein, the URTP intensity of the composite film was measured during multiple on-off switches. For URTP activation, the film was irradiated with a 400 nm light (10 mW/cm^2) for 30 s; for URTP deactivation or erasing, the film was heated at 393 K on a flat heater for 10 min. **(A)** The URTP intensity measured after each photo-activation and thermal-deactivation was plotted against repeat numbers. Over 70% URTP intensity remained within the first 40 cycles. **(B)** The URTP decay profile of the film at 1st and 40th cycle, respectively. No significant variation in decay properties was observed. **(C)** URTP emission spectra of the film measured at 1st and 40th cycle (RTP-on). No significant variation in emission wavelength were observed.

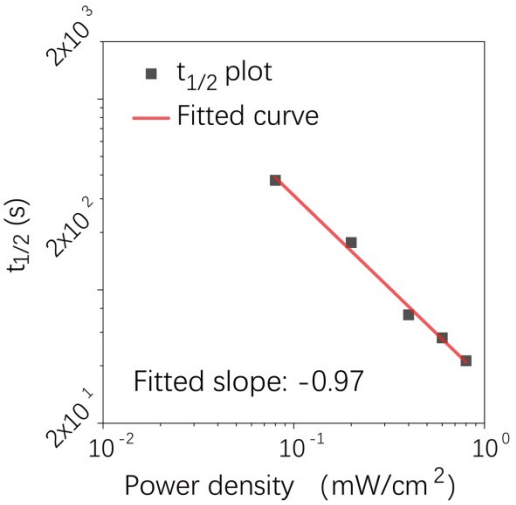

Fig. S6. Power-dependent photo-activating rate of CDs/PVP composites. To achieve different irradiation density, an optical attenuator with different transmittance (10%, 25%, 50%, 75%) was applied. The original power density of the irradiation light in the PL spectrometer (FLS 980) was measured with a PM100D Digital Handheld Optical Power and Energy Meter Console (Thorlab, America) and adjusted to 0.8 mW/cm^2 by tuning excitation silt. Resultantly, $t_{1/2}$ showed inversely proportional relationship with the irradiation power.

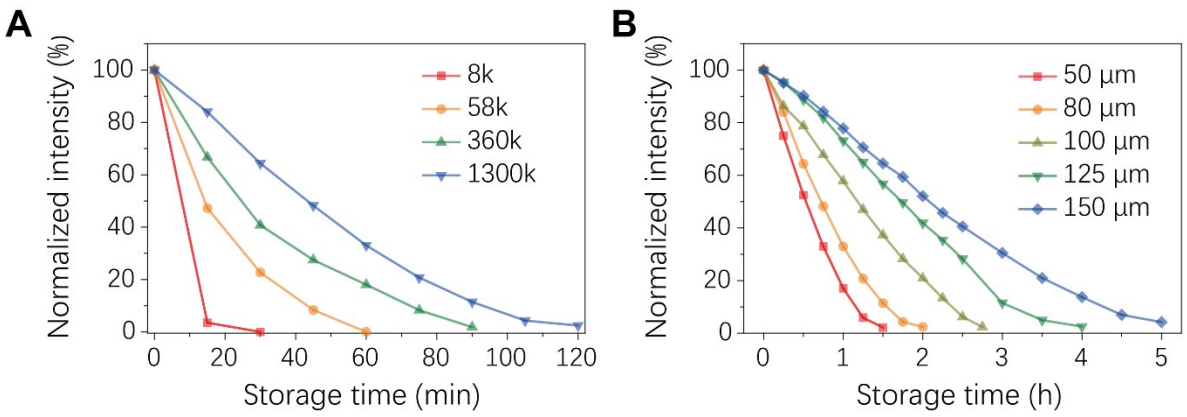

Fig. S7. Tuning of the URTP memory retention. (A) Normalized URTP intensity of CDs/PVP with different molecular weight of PVP plotted against storage time after sufficient irradiation. **(B)** Normalized URTP intensity of CDs/PVP with different thickness of PET package layer plotted against storage time after sufficient irradiation.

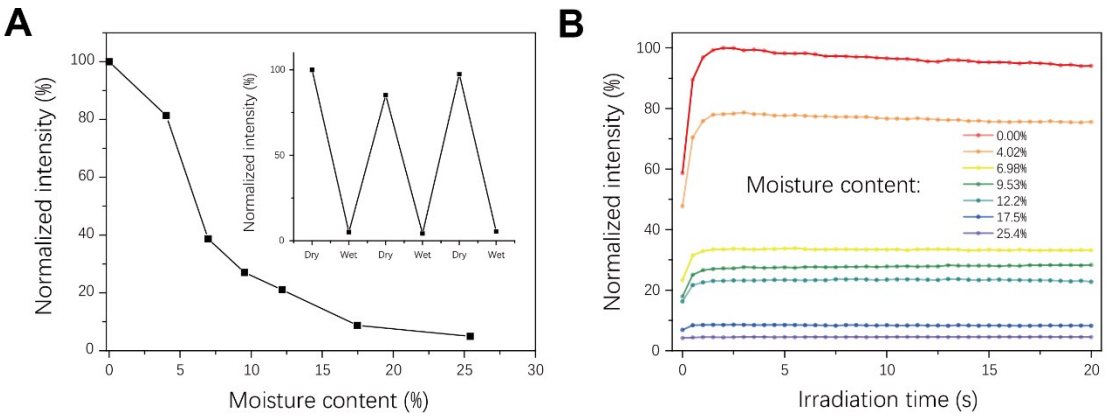

Fig. S8. Influence of moisture on the URTP emission. (A) The influence of moisture content to the URTP intensity of CDs/PVP material. The moisture content of the film was determined by weighing. **(B)** Dynamic measurement of the URTP intensities of the film with different moisture content. To exclude the influence of insufficient activation, the URTP intensities were determined by applying dynamic measurement and adopting the maximal value in each curve.

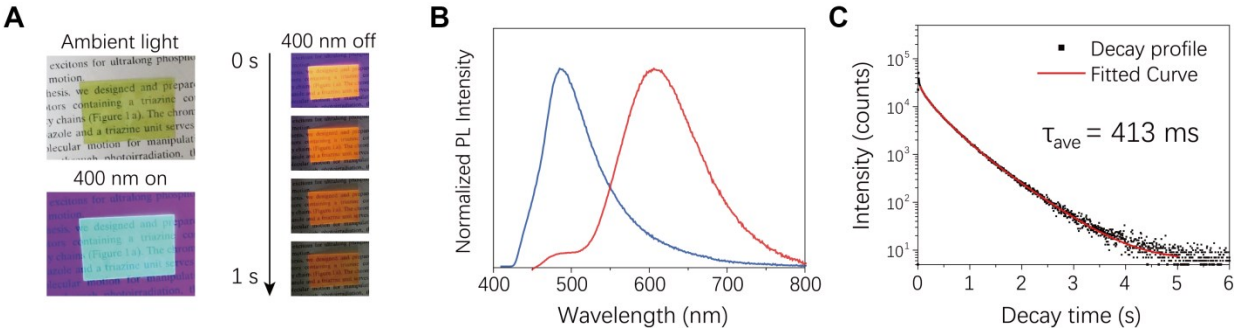

Fig. S9. The URTP properties of CDs/PAM composite. (A) Photographs of the CDs/PAM composite film under ambient light, 400 nm irradiation and after 400 nm light switched off. **(B)** The steady-state PL emission (blue line) and URTP emission spectrum (red line) of CDs/PAM composite film under 400 nm excitation. The PL steady-state emission of CDs/PAM composite peaked at 487 nm, and its delayed emission spectrum showed a maximum λ_{em} at 606 nm corresponding to URTP. Both PL and URTP emission of the CDs/PAM composite slightly red-shifted compared to that of CDs/PVP composite. **(C)** The long afterglow decay profile of CDs/PAM measured at 606 nm emission under 400 nm excitation.

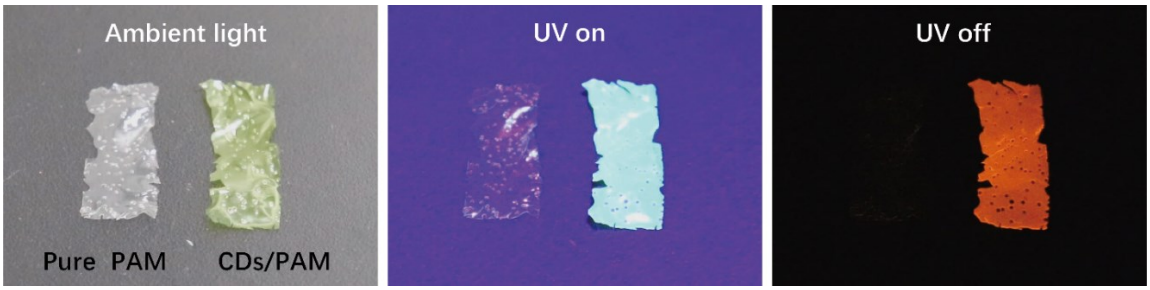

Fig. S10. Photographs of a pure PAM film and a CDs/PAM composite film under ambient light, UV irradiation and after UV irradiation just switched off. No fluorescence and long afterglow was observed from the pure PAM film.

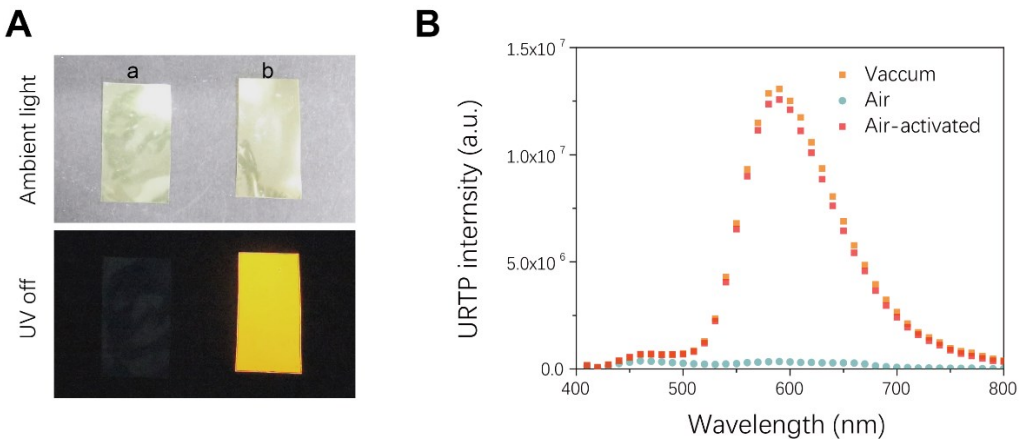

Fig. S11. The activation of URTP by vacuum degassing of CDs/PVP film. (A) Photographs of two CDs/PVP tags cut from the same film. The two tags were stored in dry air (a) and vacuum (b) for 6 h, respectively. The vacuum-degassed tag clearly showed activated long afterglow. **(B)** The URTP spectra of a CDs/PVP film after vacuum degassed (orange dots), oxygenated in air (green) and photo-activated in air (red)**.**

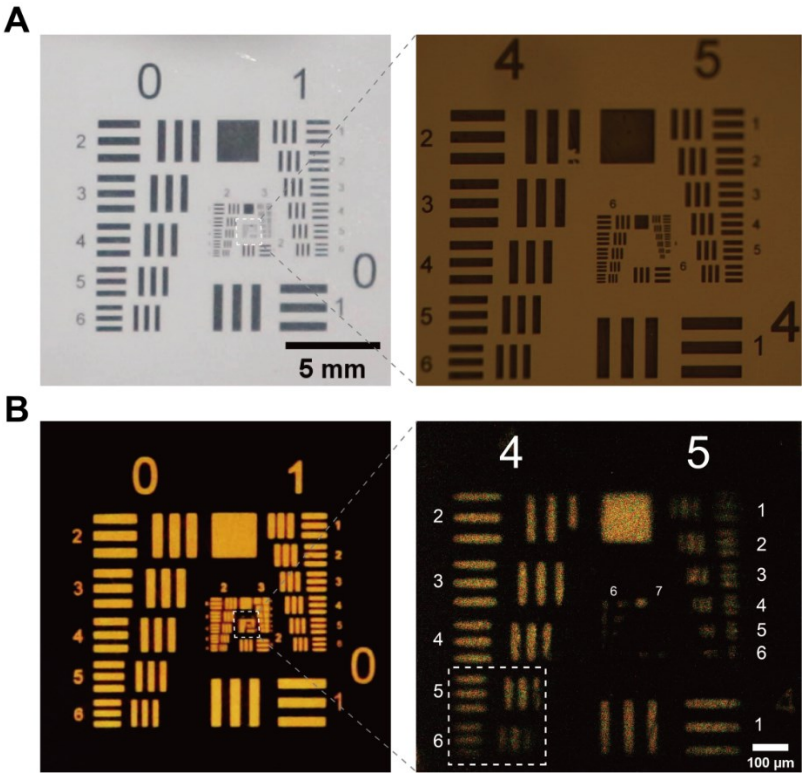

Fig. S12. Resolution determination with standard USAF-1951 test target. (A) The photographs of the standard test target under direct observation (left) and optical microscopy (right). **(B)** The miniature URTP pattern created from a by masking and lithography under direct observation (left) and optical microscopy (right). The boundary between lines started to blur in group 4, between element 5 (line width: 19.69 µm) and 6 (line width: 17.54 µm), corresponding to a limiting resolution of 1289 ~ 1451 dpi. The lines in group 5 were barely legible but the existence of all six elements was still recognizable.

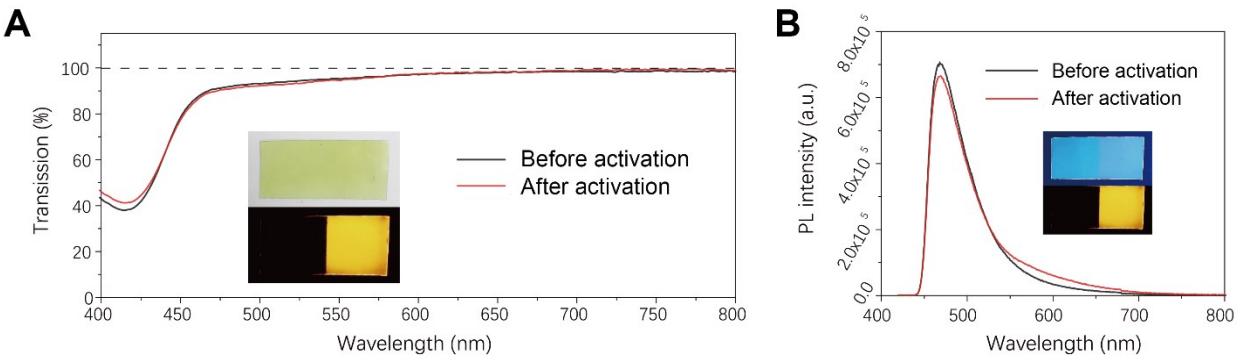

Fig. S13. The transmittance and steady-state emission features of CDs/PVP composite film before and after photo activation. (A) Visible light (400~800 nm) transmittance of the film before and after activation. (Inserted: CDs/PVP film half activated on the right side. Top: under ambient light; bottom: after UV switched off.) **(B)** PL emission of the film before and after activation. (Inserted: CDs/PVP film half activated on the right side. Top: under 400 nm UV irradiation; bottom: after UV switched off.)

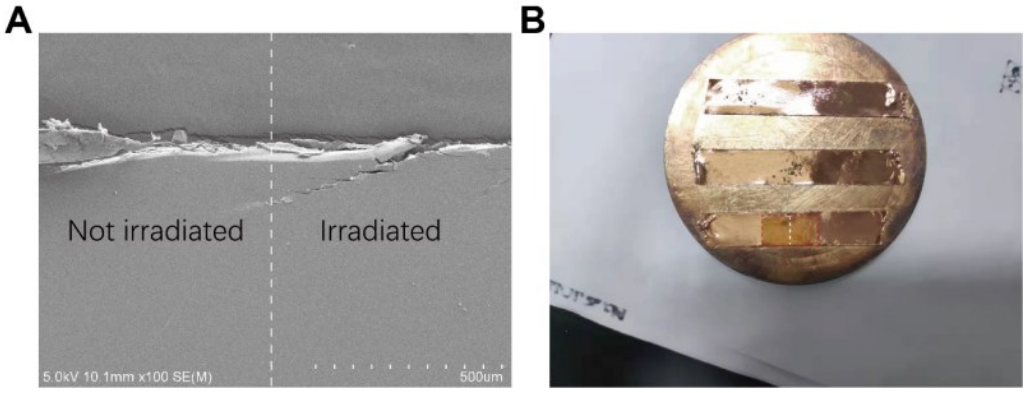

Fig. S14. The morphology of CDs/PVP composite film before and after photo-activation. (A) The SEM image of CDs/PVP composite film half activated by photo-irradication. **(B)** Photograph of the CDs/PVP composite film half activated on the right side.

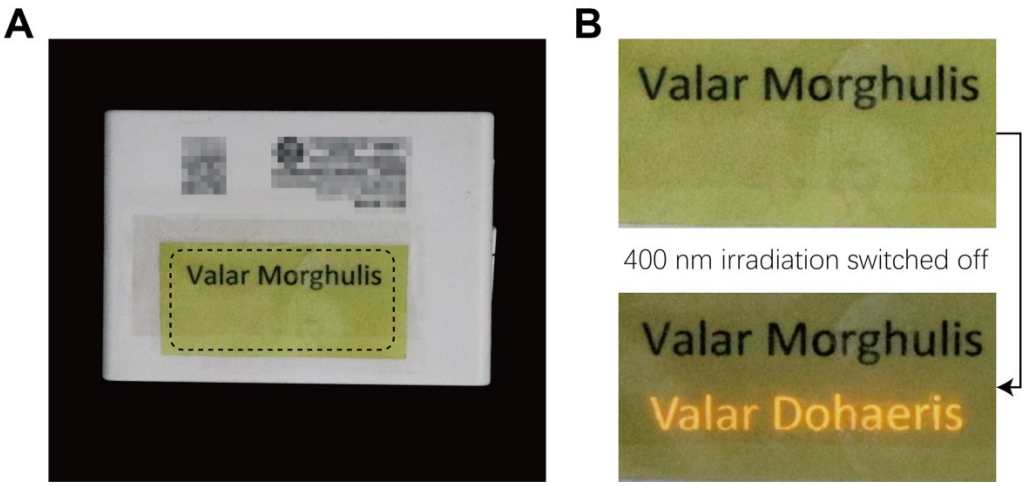

Fig. S15. Photograph of CDs/PVP labels for optical encryption. (A) Photograph of CDs/PVP tag with hidden text information attached to an object. The text printed with toner was clearly observable through the transparent film. Meanwhile, the optically-printed information remained invisible. **(B)** Photographs of the selected region (labeled with the dotted line in A) enlarged. After shortly irradiated with 400 nm lamp and switched off, the optically-printed information became observable.

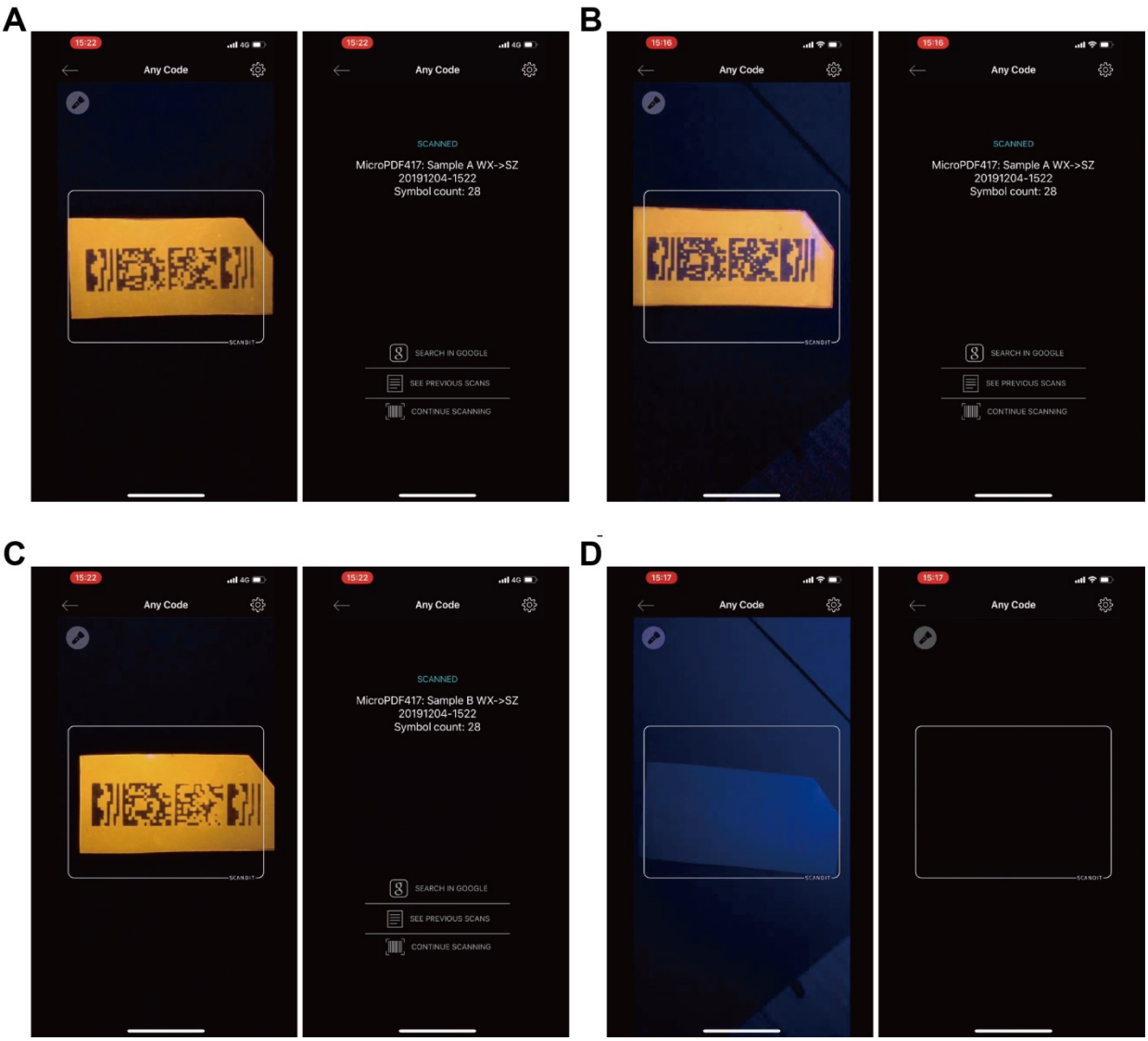

Fig. S16. The screenshots of a smartphone while scanning the editable TTI logistics labels. (A) Scanning sample A upon departure. **(B)** Scanning sample A upon arrival. **(C)** Scanning sample B upon departure. **(D)** Scanning sample B upon arrival. (In this work, an iphone X cellphone installed with an APP named *scandit* was used as the barcode reading device.)

Table S1. The peak assignments in the FT-IR spectra of CDs.

Wavenumber (cm^{-1})	Assignment	Type
3382	Amine/Hydroxyl	N-H stretch/O-H stretch
2920	Alkyl	C-H stretch
2850	Alkyl	C-H stretch
1650	Double bonds	C=C /C=O/C=N stretch (Overlapped)
1514	Alkenyl	C=C stretch
1470	Alkyl	C-H bend
1380	Amine	C-N stretch (C=C-N)
1214	Hydroxyl	C-O stretch
1100	Amine	C-N stretch (C-C-N)

Table S2. URTP lifetime fitting data of CDs/PVP composite.

Lifetime component	Lifetime value (ms)	A	Relative portion/B
τ_1	66.84	583.85	2.69%
τ_2	327.42	990.52	22.32%
τ_3	676.99	1610.03	74.99%
τ_{ave}	582.62	/	/

Table S3. URTP lifetime fitting data of CDs/PVP composite.

Lifetime component	Lifetime value [ms]	A	Relative portion/B
τ_1	70.65	6271.83	5.40%
τ_2	291.75	14100.74	50.16%
τ_3	592.4	6151.61	44.44%
τ_{ave}	413.42		/